

Strain-driven chiral phonons in two-dimensional hexagonal materials

Habib Rostami,¹ Francisco Guinea,^{2,3,4} and Emmanuele Cappelluti⁵

¹*Nordita, KTH Royal Institute of Technology and Stockholm University,
Hannes Alfvéns väg 12, 10691 Stockholm, Sweden*

²*Imdea Nanoscience, Faraday 9, 28047 Madrid, Spain*

³*Donostia International Physics Center, Paseo Manuel de Lardizábal 4, 20018 San Sebastián, Spain*

⁴*Ikerbasque. Basque Foundation for Science. 48009 Bilbao. Spain.*

⁵*Istituto di Struttura della Materia-CNR (ISM-CNR), Trieste, Italy*

Hexagonal two-dimensional materials with broken inversion symmetry (as BN or transition metal dichalcogenides) are known to sustain chiral phonons with finite angular momentum, adding a further useful degree of freedom to the extraordinary entangled (electrical, optical, magnetic and mechanical) properties of these compounds. However, because of lattice symmetry constraints, such chiral modes are constrained to the corners of the Brillouin zone, allowing little freedom for manipulating the chiral features. In this work, we show how the application of uniaxial strain leads to the existence of new chiral modes in the vicinity of the zone center. We also show that such strain-induced chiral modes, unlike the ones pinned at the K points, can be efficiently manipulated by modifying the strain itself, which determines the position of these modes in the Brillouin Zone. The results of the present paper add a new technique for the engineering of the quantum properties of two-dimensional lattices.

Introduction–. The possibility of exfoliating and/or growing two-dimensional materials at the atomically-thin level [1–7] has paved the way to designing flexible systems with a striking capability of converting mechanical deformations into electronic or optical properties [8–11]. In the paradigmatic case of graphene, as well as for other systems with a hexagonal/triangular lattice, like h-BN or transition-metal-dichalcogenides (TMDs)[12], the entanglement between electronic properties and the lattice is enriched by the presence of two inequivalent sublattices. Such additional degree of freedom is conveniently cast in term of a *spinor* vector [13] which, in the momentum space, is reflected in the occurrence of two inequivalently valleys at the high-symmetry points K, K'. The possibility of tuning the physical properties of two valleys, and encoding there quantum information, has given rise to the concept of *valleytronics* [14, 15]. A peculiar feature of the graphene, BN and TMDs, due to their hexagonal lattice symmetry, is that each valley is characterized by a remarkable chiral structure, with opposite chirality of opposite K points. Furthermore, the breaking of inversion symmetry leads to a gap opening which is accompanied by the onset of a finite Berry curvature [16–19].

Lattice modes (phonons) represent a further degree of freedom that can convey interesting quantum phenomena. Moreover, it was recently showed that also phonons in a hexagonal lattice with mass disproportion (e.g. BN or TMDs) can carry an angular momentum and sustain *chiral* modes, in the same way as electrons do. [20–29] Manipulating the properties of the lattice modes can provide thus an alternative and/or complementary scenario with promising perspectives for writing-in/reading-out quantum information.

The phonon dispersion of graphene presents a Dirac structure at the K, K' points in the subspace of the acoustic/optical modes. In similar way as for the elec-

tronic Dirac states, a key role is played by the breaking of inversion symmetry, driven by the mass disproportion, and leading to the opening of a gap at K, K'. Just as for the electronic degrees of freedom, as pointed out in the seminal work in Ref. 21, due to the crystal symmetry, such chiral phonons are pinned at the high-symmetry points K, K'. Symmetry arguments predict that chirality concepts could apply as well at the zone-center Γ point, where the degeneracy of the transverse and longitudinal modes in the Cartesian basis can be as well expressed in term of two (degenerate) chiral modes with opposite sign. Such opportunity is however not particularly useful for practical purposes since the intrinsic degeneracy of the two modes does not allow for a feasible manipulation of the chiral degree of freedom. Degeneracy splitting is thus a necessary requirement. Within this perspective, applying a real magnetic field, through the electron-phonon coupling, has been shown to induce a chiral lattice polarization [30], whereas uniaxial strain has been discussed to be detrimental with respect to chirality since it favours linear polarization [31–34]. Finding the way of sustaining chiral modes in the closeness of the Γ point is thus of the highest relevance since it could open the way for a direct probe of chiral phonons by means of optical means at $\mathbf{q} \approx 0$.

In this work we demonstrate that novel chiral phonons can be conveniently generated and engineered close to the Γ point in the optical branches of hexagonal systems with sublattice inequivalence (e.g. h-BN, TMDs, gapped graphene) by applying simple homogeneous uniaxial strain. Furthermore, we show that such new chiral modes appear in pairs of opposite chirality, and, unlike the chiral modes constrained at the K, K' point, the net momentum for each chirality does not average to zero. The closeness of the chiral phonons to the Γ point on the other hand opens the way for an optical probe.

Strain-driven chiral phonon modes-. For a closer comparison with previous literature, we begin considering the paradigmatic case of a hexagonal lattice with interatomic distance a and two different masses M_1 , M_2 in the two sublattices (see Fig. 1a). The corresponding Brillouin zone is also shown in Fig. 1b. The elastic properties are described by means of a nearest-neighbor force-constant model with a radial spring constant ϕ_r and a transverse (in-plane) constant ϕ_t . Following a standard derivation in literature (see Supplementary Material for further details [35]), the lattice modes are ruled by the dynamical matrix [36] which can be written as:

$$\hat{D}(\mathbf{q}) = \begin{pmatrix} \hat{G}/M_1 & \hat{F}_{\mathbf{q}}/\sqrt{M_1M_2} \\ \hat{F}_{\mathbf{q}}^*/\sqrt{M_1M_2} & \hat{G}/M_2 \end{pmatrix}, \quad (1)$$

where $\hat{G} = \sum_{i=1}^3 \hat{\Phi}_i$, $F_{\mathbf{q}} = -\sum_{i=1}^3 \hat{\Phi}_i e^{i\mathbf{q}\cdot\delta_i}$, and where $\hat{\Phi}_1 = \text{diag}[\phi_r, \phi_t]$ and $\hat{\Phi}_2 = \hat{R}^\dagger(\theta_0)\hat{\Phi}_1\hat{R}(\theta_0)$ and $\hat{\Phi}_3 = \hat{R}^\dagger(-\theta_0)\hat{\Phi}_1\hat{R}(-\theta_0)$. Here $\hat{R}(\theta_0)$ represents the rotation matrix around the z -axis with $\theta_0 = 2\pi/3$. In the following, in order to better show the novel results of our work, we use the same force constant parameters employed in Ref. 21, $\phi_r = 1$, $\phi_t = 0.25$, with a atomic mass difference $M_1 = 1$, $M_2 = 3$ that reproduces qualitatively the case of MoS₂.

The eigenvalues of the dynamical matrix provide the phonon dispersion $\omega_\lambda(\mathbf{q})$ whereas the eigenvectors $\epsilon_\lambda(\mathbf{q})$ rule the lattice displacements and carry the information about the chiral character. This can be captured by switching the representation of the lattice displacements from the Cartesian basis $|x_1\rangle$, $|y_1\rangle$, $|x_2\rangle$, $|y_2\rangle$, to the chiral basis defined by the $|R_\alpha\rangle = (|x_\alpha\rangle + i|y_\alpha\rangle)/\sqrt{2}$, $|L_\alpha\rangle = (|x_\alpha\rangle - i|y_\alpha\rangle)/\sqrt{2}$, ($\alpha = 1, 2$). It is thus convenient to introduce the phonon circular polarization [21, 35], defined as

$$s_{z,\lambda}(\mathbf{q}) = \sum_{\alpha=1,2} (|\epsilon_{R,\alpha,\lambda}(\mathbf{q})|^2 - |\epsilon_{L,\alpha,\lambda}(\mathbf{q})|^2), \quad (2)$$

where $\epsilon_{R/L,\alpha,\lambda}$ are the phonon eigenvectors of the dynamical matrix expressed in the chiral basis. The phonon circular polarization is strictly related to the phonon orbital angular momentum, which can be defined for each phonon band as $L_{z,\lambda}(\mathbf{q}) = \hbar s_{z,\lambda}(\mathbf{q}) \{n_B[\omega_\lambda(\mathbf{q})/T] + 1/2\}$, where $n_B[x] = 1/[\exp(x) - 1]$ if the Bose-Einstein factor.

The phonon dispersion displays four bands (we number them $\lambda = 1, \dots, 4$, from lower to higher energies) with two optical branches degenerate at Γ with E_{2g} symmetry and two acoustic branches. In agreement with Ref. 21, for the perfect hexagonal lattice, we find chiral modes with opposite chirality at the K, K' points for bands 2 and 3. An inspection of the eigenvectors show that such chiral modes have a pure-sublattice character, with the mode of band 2 (3) involving chiral lattice displacements only of the heavier (lighter) sublattice.

We will show that new physics and new chiral modes appear upon applying an anisotropic strain, described

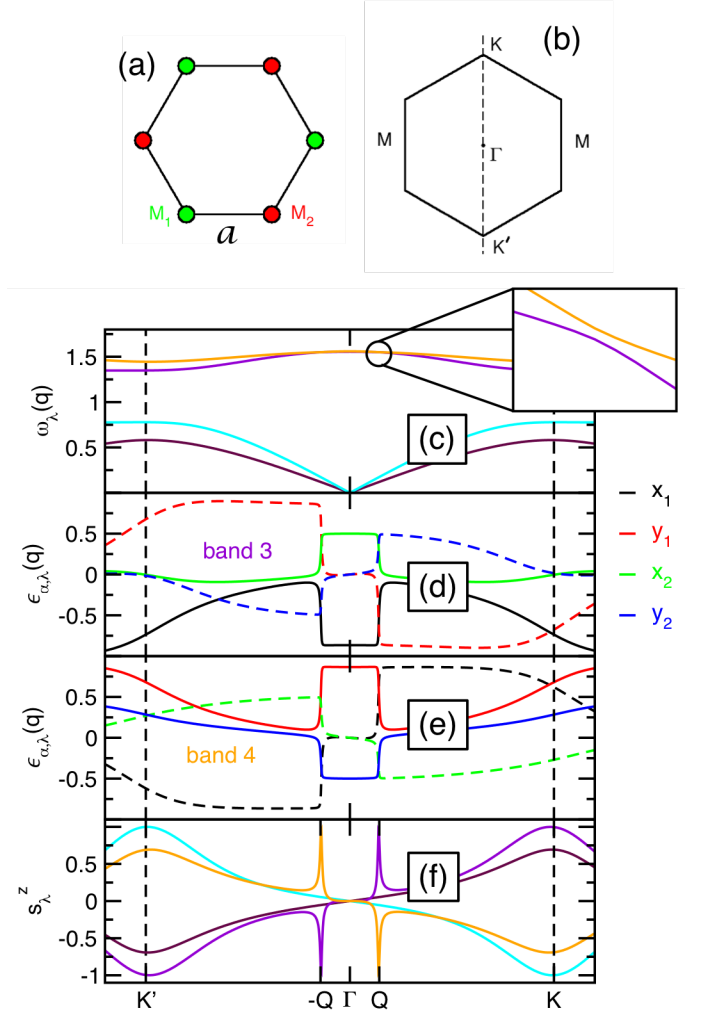


FIG. 1. (a) Lattice structure and (b) Brillouin zone of a bipartite hexagonal lattice. Atoms on the sublattice 1 have masses M_1 , atoms on the sublattice 2 have masses M_2 . (c) Phonon dispersion along the cut K'- Γ -K for the force-constant model described in the text, upon an uniaxial tensile strain $\epsilon_+ = 2\%$ along the x direction. Brown, cyan, violet and orange lines denote phonon bands from $\alpha = 1, \dots, 4$, respectively. Inset: a magnification of the region close to the avoided-band-crossing point Q. (d)-(e) Corresponding eigenvectors of the lattice displacements of band 3 and 4. Black, red, green and blue lines show the normalized lattice displacement along x_i and y_i for atom i . Solid lines represent the real component, whereas dashed lines denote the imaginary part. (f) Corresponding phonon circular polarization $s_{z,\lambda}$ for all the four bands. Color code as in panel (c).

by the strain tensor $\epsilon_{ij} = (\partial_i u_j + \partial_j u_i)/2$, where $\partial_i u_j$ is derivative of the *strain* lattice displacement u_j along the direction i [37]. On general ground, the above tensor can be viewed as a combination, an isotropic biaxial average strain $\epsilon_0 = (\epsilon_{xx} + \epsilon_{yy})/2$, of a tensile ($\epsilon_+ > 0$) and a compressive ($\epsilon_- > 0$) orthogonal components, aligned

along the angles [38]

$$\theta_+ = \theta_- + \frac{\pi}{2} = \frac{1}{2} \arctan \left(\frac{2\varepsilon_{xy}}{\varepsilon_{xx} - \varepsilon_{yy}} \right), \quad (3)$$

and with respective strain values $\varepsilon_{\pm} = \varepsilon_0 \pm \Delta\varepsilon/2$, where

$$\Delta\varepsilon = \sqrt{(\varepsilon_{xx} - \varepsilon_{yy})^2 + 4\varepsilon_{xy}^2}. \quad (4)$$

Within the framework of a force-constant analysis, anisotropic in-plane strain affects the phonon properties through two main effects: (i) the elongation/compression of the bonds, tuning the spring constants $\phi_r(R)$, $\phi_t(R)$ whose values depend intrinsically on the interatomic distance R ;— similar to the case of hopping energies in electronic tight-binding models [39–45] (ii) the geometrical change of the angles between neighbor atoms, implying different mixing of the x and y components of the lattice displacements. For the sake of completeness, we retain both effects, although each of them, separately, is sufficient to generate new chiral modes. The mathematical implementation of anisotropic strain within the force-constant model follows a straightforward procedure and we refer to the Supplementary Material for technical details [35].

In Fig. 1c we show the phonon dispersion along the vertical cut $K'-\Gamma-K$ (see panel b) for an uniaxial tensile strain $\varepsilon_+ = 2\%$ ($\varepsilon_- = 0$) along the x (armchair) direction ($\theta_+ = 0$). We label the bands as $\lambda = 1, \dots, 4$, from lower to higher energies. At the Γ point ($\mathbf{q} = 0$) we observe the well-known splitting of the E_{2g} phonons in two non-degenerate modes $\omega_{\Gamma-}$, $\omega_{\Gamma+}$ ($\omega_{\Gamma-} < \omega_{\Gamma+}$) with eigenvectors aligned along θ_+ , θ_- . As a general rule the softer mode $\omega_{\Gamma-}$ corresponds to lattice displacements along the tensile axis θ_+ of strain direction (in this case the x direction), while the harder mode $\omega_{\Gamma+}$ is associated with the compressive strain along θ_- . Such splitting, for the tensile strain along x , implies a “band crossing” at momenta $\pm Q$ along the y -axis $K'-\Gamma-K$ cut based on the simple model here considered with transverse-optical (TO) modes harder than the longitudinal-optical (LO) ones [46].

A closer look at the phonon dispersion (see inset of Fig. 1c) shows however that such “phonon-band-crossing” is however just apparent but it is actually an “avoided-band-crossing” with a finite gap $\Delta\omega_{\text{chi}}$ between the two phonon branches. A deeper understanding of the physics here at work can be attained from the analysis of the phonon mode eigenvectors $\epsilon_{\alpha,\lambda}(\mathbf{q})$ (Fig. 1d,e). As expected, close to the Γ point, in the strained case, band 3 and band 4 are characterized by lattice displacements almost purely aligned along x and y respectively, with atom 2 moving counter-phase versus atom 1. The opposite occurs of course for momenta larger than the “crossing” point, where the order of the bands is reversed. A true band-crossing would happen if the eigenvectors would be purely real. However, at finite momenta, a small imaginary component is always unavoidably present. The

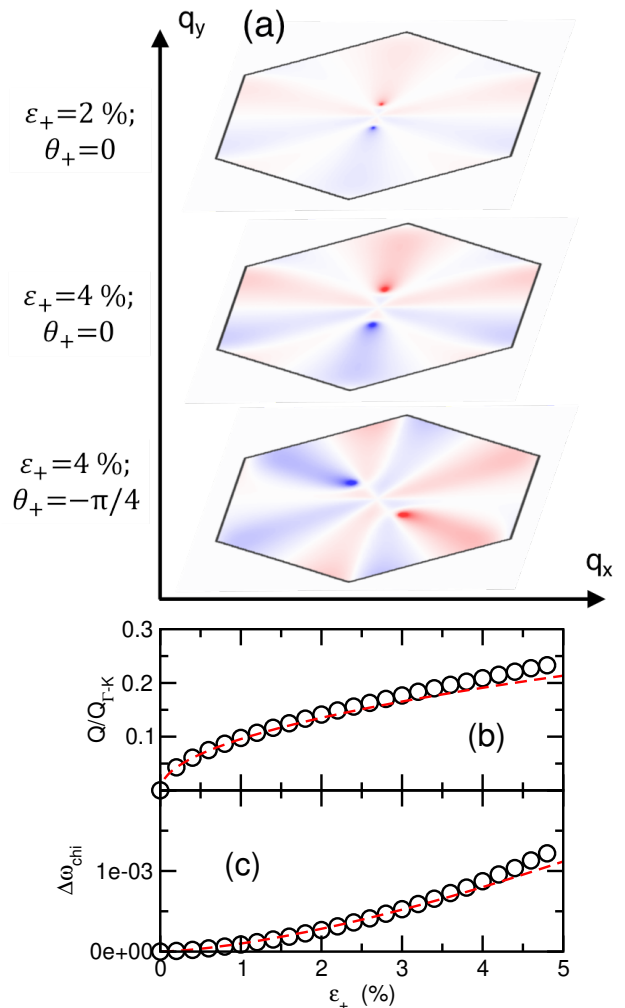


FIG. 2. (a) Color map of $\Delta s_{z,\lambda}$ for the optical phonon band 4 upon different values and directions of applied strain. Red and blue regions represent positive and negative phonon circular polarizations, respectively. Panels (b)-(c): dependence of crossing point Q and of the phonon gap $\Delta\omega_{\text{chi}}$ on the strain magnitude for the top case shown in panel (a). Black symbols represent results using the full force-constant model; the dashed red line using the two-band model.

presence of such finite imaginary part prevents a true crossing, expected between bands with orthogonal lattice displacements, and the switch between the lattice displacements of band 3 for $|q_y| \leq Q$ and band 4 for $|q_y| \geq Q$ occurs through a sudden *chiral twist* where the real x component acquires an imaginary y component and vice versa. Right at the momentum of the avoided-crossing point, $\mathbf{q} = \pm Q$, the eigenmodes of band 3 and 4 are described exactly by the chiral basis. This is remarkably shown in Fig. 1f where we illustrate the phonon circular polarization for each phonon band. Here we can clearly see that, besides the well-known chiral phonons at K , K' , in bands 2 and 3, *new* chiral phonons appear upon anisotropic strain in bands 3 and 4 close to the Γ

point, with opposite circular phonon polarization at $\pm Q$. It is worth to stress here that such novel chiral phonons present striking different properties with respect to the standard chiral phonon pointed out in Refs. [21, 23]. Indeed, while chiral phonons discussed in Refs. [21, 23] are locked at the high-symmetry points K, K' at the edge of the Brillouin zone, and they obey a threefold symmetry, the chiral phonons arising upon anisotropic strain have a *tunable* location in the Brillouin zone controlled by the strength and by the direction of the strain. Since for vanishing strain $|\varepsilon| \rightarrow 0$ the \mathbf{q} -momentum of such chiral phonon approaches zero, $|\mathbf{Q}| \rightarrow 0$, for small strain these phonons are expected to appear close to the Γ point, where spectroscopic optical probes can be effective.

Low-energy description-. In order to highlight the role of the anisotropic strain, we analyze for each phonon band the change in the phonon circular polarization induced by the anisotropic strain, namely $\Delta s_{z,\lambda} = s_{z,\lambda}(\hat{\varepsilon}) - s_{z,\lambda}(\hat{\varepsilon} = 0)$. The tunability of such new chiral phonons by means of strain is shown in Fig. 2a where we plot in a color map $\Delta s_{z,\lambda}$ of the optical phonon band $\lambda = 4$ for different magnitudes and directions of the applied strain. We see that increasing strain shifts the momentum $\pm \mathbf{Q}$ of chiral phonons at larger values, whereas the presence of a shear component rotates \mathbf{Q} away from the crystallographic axes. As a general rule, the couple of such strain-induced chiral phonons, with opposite circular phonon polarization, appears along the direction in the reciprocal space *perpendicular* to the strain tensile component in real space.

The dependence of \mathbf{Q} on the strain magnitude is shown in Fig. 2b, while in panel c we plot the value of the phonon gap $\Delta\omega_{\text{chi}}$ between band 4 and 3. A full control and prediction of the properties of such new chiral phonons upon strain can be analytically achieved by introducing an effective reduced model. To this aim we employ a Schrieffer-Wolf transformation restricted to the relevant bands 3 and 4, which are described at the Γ point by counter phase displacements (along x and y) of atoms 1 and 2 with a weight dictated by the masses: $\epsilon_3(\Gamma) = (1/\sqrt{M_1}, 0, -1/\sqrt{M_2}, 0)$, $\epsilon_4(\Gamma) = (0, 1/\sqrt{M_1}, 0, -1/\sqrt{M_2})$. Technical details are reported in the Supplementary Material [35]. In such 2×2 Hilbert space it is convenient to work directly in the chiral basis, $v_L = (v_3 + iv_4)/\sqrt{2}$, $v_R = (v_3 - iv_4)/\sqrt{2}$. The resulting phonon properties at the linear order in strain are described thus by the dynamical matrix $\hat{D}_0(\mathbf{q}) + D_\varepsilon(\mathbf{q})$. Here $\hat{D}_0(\mathbf{q})$ accounts for the lattice properties in the absence of strain, while $D_\varepsilon(\mathbf{q})$ contains the corrections due to an anisotropic strain. More explicitly, close to the Γ point, we have

$$\hat{D}_0(\mathbf{q}) = \omega_\Gamma^2 \begin{pmatrix} 1 - a_0|\mathbf{q}|^2 & a_1 q_L^2 \\ a_1 q_R^2 & 1 - a_0|\mathbf{q}|^2 \end{pmatrix}, \quad (5)$$

where $q_{L/R} = q_x \pm iq_y$, and where $a_0 = 0.077$, $a_1 = 0.028$ are the relevant parameters of such $\mathbf{k} \cdot \mathbf{p}$ -like expansion

for the phonon bands. The numerical value of a_0 , a_1 is dictated by the microscopical parameters ϕ_r , ϕ_t , M_1 , M_2 and their analytical expression is provided in the Supplementary Material [35].

The resulting phonon bands in unstrained case are described thus by $\omega_\pm(\mathbf{q}) = \gamma_\pm(\mathbf{q})\omega_\Gamma$ where $\gamma_\pm^2(\mathbf{q}) = 1 - (a_0 \pm a_1)|\mathbf{q}|^2$. The strain correction term on the other hand can be computed at the leading order in the $\mathbf{q} \rightarrow 0$ limit and it reads:

$$\hat{D}_\varepsilon(\mathbf{q} = 0) = \omega_\Gamma^2 \begin{pmatrix} -2\alpha_0\varepsilon_0 & \alpha_1\varepsilon_R \\ \alpha_1\varepsilon_L & -2\alpha_0\varepsilon_0 \end{pmatrix}, \quad (6)$$

where $\varepsilon_{L/R} = \varepsilon_{xx} - \varepsilon_{yy} \pm i2\varepsilon_{xy}$, $\alpha_0 = 1.5$ and $\alpha_1 = 0.15$. The phonon bands computed by diagonalizing $\hat{D}_0(\mathbf{q}) + D_\varepsilon(0)$ read thus $\omega_\pm(\mathbf{q}) = \gamma_{\pm,\varepsilon}(\mathbf{q})\omega_\Gamma$, where

$$\gamma_{\pm,\varepsilon}^2(\mathbf{q}) = 1 - a_0|\mathbf{q}|^2 - 2\alpha_0\varepsilon_0 \pm \sqrt{[a_1(q_x^2 - q_y^2) - \alpha_1(\varepsilon_{xx} - \varepsilon_{yy})]^2 + 4[a_1q_xq_y + \alpha_1\varepsilon_{xy}]^2}. \quad (7)$$

Note that, although the parameters a_i , α_i can be as well easily evaluated within the minimal nearest-neighbor force-constant model (see Supplementary Material), the validity of Eqs. (5)-(7) holds true in full generality for realistic phonon bands where the parameters a_i , α_i can be extracted from first-principle calculations and/or from direct experimental probes. Within the present framework, limited to a quadratic expansion in \mathbf{q}^2 , we can now analytically identify the momentum Q where a band anticrossing occurs and chiral phonons appears. For the teachful example of uniaxial tensile strain along the x direction, $\varepsilon_+ \neq 0$, $\varepsilon_- = 0$, $\theta_+ = 0$, we find $Q_x = 0$, $Q_y = \pm\sqrt{\alpha_1\varepsilon_+/a_1}$, in perfect agreement with the numerical results for the full phonon band dispersion (Fig. 1c). For generic case, including shear strain, we find that the momentum $\mathbf{Q}_\pm = \pm Q(\cos\phi, \sin\phi)$ is univocally determined by the strain tensor, with the angle ϕ aligned along the compression direction, $\phi = \theta_-$, and Q^2 being determined by the strain difference between the two main components:

$$Q^2 = \left| \frac{\alpha_1}{a_1} \right| \Delta\varepsilon. \quad (8)$$

It is worth to mentioning that, in addition to the above analysis, using in Eq. (5)-(6) an expansion for small strains hence small \mathbf{q} 's, is very efficient in determining the location of the new chiral modes, but it also predicts a *true* phonon band crossing, with two degenerate modes at \mathbf{Q} , not a well-defined chiral character. A true gap, and thus a robust chiral character, is recovered however in a more realistic modelling when a higher order dependence on the momenta is retained. From a dimensional analysis, since $|Q|$ scales with the square root of the strain amplitude, one can realize that the next leading order effects are driven by the cubic \mathbf{q}^3 terms in Eq.

(5), which lead to a correction $\hat{D}_0(\mathbf{q}) \rightarrow \hat{D}_0(\mathbf{q}) + \hat{D}_1(\mathbf{q})$ where $\hat{D}_1(\mathbf{q}) \propto A|\mathbf{q}|^3\hat{\sigma}_3$. The gap $\Delta\omega_{\text{chi}}$ between the two new chiral modes appearing under strain is predicted thus to behave as $\Delta\omega_{\text{chi}} \propto (\Delta\varepsilon)^{3/2}\sin(3\phi)$. The strain dependence of the gap $\Delta\omega_{\text{chi}} = \omega_+(\mathbf{Q}) - \omega_-(\mathbf{Q})$ between the two chiral modes is also shown in Fig. 2c by comparing the numerical results obtained by the effective phonon dispersion evaluated with the force-constant model with the effective two-band model. Once again we find a striking agreement.

It should be stressed the role of the gap $\Delta\omega_{\text{chi}}$. Indeed, like for the chiral modes at the K points, it is the presence of such gap that makes the chiral modes physically observable. Assuming for characteristic two-dimensional systems (BN, TMDs) that the frequency of the optical modes lies in the range $\omega_{\Gamma} \approx 300 - 1400 \text{ cm}^{-1}$ [47–52], and considering realistic values of the strain, the gap can be of the order of a fraction or one cm^{-1} , beyond the possibility of a spectroscopy probe. Alternatively, the effect of such strain-induced chiral modes might be detected in macroscopic quantities, through the different populations $n_{\text{B}}[\omega_+(\mathbf{Q})/T] \neq n_{\text{B}}[\omega_-(\mathbf{Q})/T]$, where T is the temperature. It should be noticed indeed that, due to such new chiral modes, the system acquires a finite “chiral wavevector” defined as $\bar{\mathbf{Q}} = \sum_{\lambda, \alpha_{\pm}} \mathbf{Q}_{\alpha} s_{z, \lambda}(\mathbf{Q}_{\alpha}) n_{\text{B}}[\omega_{\lambda}(\mathbf{Q}_{\alpha})]$. This is significantly different from the chiral modes at the K points in the absence of strain where the threefold symmetry enforces $\bar{\mathbf{Q}} = 0$. The temperature, which has here a clear relevant role ruling the finite different population, should be compared with the optical phonon frequencies $\omega_{\Gamma} \approx \omega_+(\mathbf{Q}), \omega_-(\mathbf{Q})$. At room temperature such ratio is still quite small, preventing probably a direct experimental probe of $\bar{\mathbf{Q}}$. Interesting perspectives could be prompted however from time-resolved pump-probe approaches. A common trait of two-dimensional hexagonal materials is indeed that pump-induced energy, initially stored in the electronic degrees of freedom, can be quickly transfer to few lattice modes, corresponding to intravalley and intervalley scattering. Those modes (including \mathbf{Q}_{α}) can thus get *hot*, with effective temperatures that can reach the order to 10^3 K , making the possibility of probing the effects of a finite $\bar{\mathbf{Q}}$ more accessible. Further promising scenarios can come from near-field optical techniques, where finite \mathbf{q} optical excitations can be launched, and couple to the chiral phonons considered here. Tuning the near-field conditions to better probe $\mathbf{q} \approx \mathbf{Q}_{\alpha}$, with a circular polarized light, might be efficiently result in selectively exciting phonon modes with a specific chirality.

A final mention concerning the possible ways of probing the new (strain-driven) chiral phonons at small \mathbf{q} 's is through their effect on the acoustic modes. As discussed above, at \mathbf{Q}_{α} the physics of the avoided crossing point is strictly reflected in the optical branches, inducing modes with opposite chiralities $s_{z, 3/4}(\mathbf{Q}_{\alpha}) \approx \pm 1$. However, a small but sizable chirality content is present at \mathbf{Q}_{α}

also in the acoustic branches, with $s_{z, 1}(\mathbf{Q}_{\alpha}) \approx -0.16$ and $s_{z, 2}(\mathbf{Q}_{\alpha}) \approx 0.15$, with a net $s_{z, 1}(\mathbf{Q}_{\alpha}) + s_{z, 2}(\mathbf{Q}_{\alpha}) \approx -0.01$. Although clearly less strong than in the optical branches, it should keep in mind that such difference applies to modes that are *strongly* non degenerate. Furthermore, the low-energy of the acoustic lattice modes makes them easily thermally populated and highly relevant for the transport properties. The strain-induced chirality might be thus feasibly probed through the macroscopical effects related to the small but finite chiral content of the acoustic modes.

Acknowledgements. This work was supported by Nordita and the Swedish Research Council (VR 2018-04252). F. G. acknowledges funding from the European Commission, under the Graphene Flagship, Core 3, grant number 881603, and by the grants NMat2D (Comunidad de Madrid, Spain), SprQuMat and SEV-2016-0686, (Ministerio de Ciencia e Innovación, Spain).

-
- [1] K. Novoselov, A. Geim, S. Morozov, D. Jiang, Y. Zhang, S. Dubonos, I. Grigorieva, and A. Firsov, *Science* **306**, 666 (2004).
 - [2] K. Novoselov, D. Jiang, F. Schedin, T. Booth, V. Khotkevich, S. Morozov, and A. Geim, *Proc. Nat. Ac. Sci. Ac.* **102**, 10451 (2005).
 - [3] K. F. Mak, C. Lee, J. Hone, J. Shan, and T. F. Heinz, *Phys. Rev. Lett.* **105**, 136805 (2010).
 - [4] A. Splendiani, L. Sun, Y. Zhang, T. Li, J. Kim, C.-Y. Chim, G. Galli, and F. Wang, *Nano Lett.* **10**, 1271 (2010), pMID: 20229981.
 - [5] S. Z. Butler, S. M. Hollen, L. Cao, Y. Cui, J. A. Gupta, H. R. Gutiérrez, T. F. Heinz, S. S. Hong, J. Huang, A. F. Ismach, E. Johnston-Halperin, M. Kuno, V. V. Plashnitsa, R. D. Robinson, R. S. Ruoff, S. Salahuddin, J. Shan, L. Shi, M. G. Spencer, M. Terrones, W. Windl, and J. E. Goldberger, *ACS Nano* **7**, 2898 (2013).
 - [6] P. Ajayan, P. Kim, and K. Banerjee, *Phys. Today* **69**, 38 (2016).
 - [7] X. Li, L. Tao, Z. Chen, H. Fang, X. Li, X. Wang, J.-B. Xu, and H. Zhu, *Appl. Phys. Rev.* **4**, 021306 (2017).
 - [8] M. Vozmediano, M. Katsnelson, and F. Guinea, *Phys. Rep.* **496**, 109 (2010).
 - [9] S. Bertolazzi, J. Brivio, and A. Kis, *ACS Nano* **5**, 9703 (2011).
 - [10] R. Roldán, A. Castellanos-Gomez, E. Cappelluti, and F. Guinea, *J. Phys.: Condens. Matter* **27**, 313201 (2015).
 - [11] B. Amorim, A. Cortijo, F. de Juan, A. Grushin, F. Guinea, A. Gutiérrez-Rubio, H. Ochoa, V. Parente, R. Roldán, P. San-Jose, J. Schiefele, M. Sturla, and M. Vozmediano, *Phys. Rep.* **617**, 1 (2016).
 - [12] The crystal structure of single-layer MX_2 TMDs can be viewed from the top as an hexagonal lattice, i.e. a triangular lattice with a proper basis defined by M on the sublattice A and the top/bottom X atoms on the sublattice B.
 - [13] A. H. Castro Neto, F. Guinea, N. M. R. Peres, K. S. Novoselov, and A. K. Geim, *Rev. Mod. Phys.* **81**, 109 (2009).

- [14] S. Tarasenko and E. Ivchenko, *Jetp Lett.* **81**, 231 (2005).
- [15] A. Rycerz, J. Tworzyczo, and C. Beenakker, *Nat. Phys.* **3**, 172 (2007).
- [16] T. Ando, Y. Zheng, and H. Suzuura, *J. Phys. Soc. Jpn* **71**, 1318 (2002).
- [17] D. Xiao, W. Yao, and Q. Niu, *Phys. Rev. Lett.* **99**, 236809 (2007).
- [18] D. Xiao, M.-C. Chang, and Q. Niu, *Rev. Mod. Phys.* **82**, 1959 (2010).
- [19] T. Ando, *J. Phys. Soc. Jpn* **84**, 114705 (2015).
- [20] L. Zhang and Q. Niu, *Phys. Rev. Lett.* **112**, 085503 (2014).
- [21] L. Zhang and Q. Niu, *Phys. Rev. Lett.* **115**, 115502 (2015).
- [22] H. Zhu, J. Yi, M.-Y. Li, J. Xiao, L. Zhang, C.-W. Yang, R. A. Kaindl, L.-J. Li, Y. Wang, and X. Zhang, *Science* **359**, 579 (2018).
- [23] H. Chen, W. Zhang, Q. Niu, and L. Zhang, *2D Mater.* **6**, 012002 (2019).
- [24] W. Zhang, A. Srivastava, X. Li, and L. Zhang, *Phys. Rev. B* **102**, 174301 (2020).
- [25] H. Komiyama and S. Murakami, *Phys. Rev. B* **103**, 214302 (2021).
- [26] H. Chen, W. Wu, J. Zhu, S. A. Yang, and L. Zhang, *Nano Lett.* **21**, 3060 (2021).
- [27] A. Ptok, A. Kobińska, M. Sternik, J. Łażewski, P. T. Jochym, A. M. Oleś, S. Stankov, and P. Piekarczyk, *Phys. Rev. B* **104**, 054305 (2021).
- [28] H. Pirie, S. Sadhuka, J. Wang, R. Andrei, and J. E. Hoffman, *Phys. Rev. Lett.* **128**, 015501 (2022).
- [29] The possible onset of chiral phonons on a square lattice has been discussed in Wang *et al.*, arXiv:2111.05010 (2021).
- [30] J. Sonntag, S. Reichardt, B. Beschoten, and C. Stampfer, *Nano Lett.* **21**, 2898 (2021).
- [31] M. Huang, H. Yan, C. Chen, D. Song, T. F. Heinz, and J. Hone, *Proc. Nat. Ac. Sci.* **106**, 7304 (2009).
- [32] T. M. G. Mohiuddin, A. Lombardo, R. R. Nair, A. Bonetti, G. Savini, R. Jalil, N. Bonini, D. M. Basko, C. Galiotis, N. Marzari, K. S. Novoselov, A. K. Geim, and A. C. Ferrari, *Phys. Rev. B* **79**, 205433 (2009).
- [33] Y. Wang, C. Cong, C. Qiu, and T. Yu, *Small* **9**, 2857 (2013).
- [34] D. Doratotaj, J. R. Simpson, and J.-A. Yan, *Phys. Rev. B* **93**, 075401 (2016).
- [35] Supplementary Material is available in the attached file.
- [36] M. Born and K. Huang, *Dynamical Theory of Crystal Lattices* (Oxford University Press, 1998).
- [37] S. Timoshenko and S. Woinowsky-Krieger, *Theory of Plates and Shells* (Mc Graw Hill, 2010).
- [38] This expression is technically valid only for $\varepsilon_{xx} > \varepsilon_{yy}$. For generic strain one should replace $\arctan(y/x)$ with $\arctan2(x, y) = -i \ln[(x + iy)/\sqrt{x^2 + y^2}]$.
- [39] C. L. Kane and E. J. Mele, *Phys. Rev. Lett.* **78**, 1932 (1997).
- [40] H. Suzuura and T. Ando, *Phys. Rev. B* **65**, 235412 (2002).
- [41] K.-i. Sasaki, Y. Kawazoe, and R. Saito, *Progress of Theoretical Physics* **113**, 463 (2005).
- [42] M. Vozmediano, M. Katsnelson, and F. Guinea, *Physics Reports* **496**, 109 (2010).
- [43] E. Mariani, A. J. Pearce, and F. von Oppen, *Phys. Rev. B* **86**, 165448 (2012).
- [44] H. Rostami and R. Asgari, *Phys. Rev. B* **88**, 035404 (2013).
- [45] H. Rostami, R. Roldán, E. Cappelluti, R. Asgari, and F. Guinea, *Phys. Rev. B* **92**, 195402 (2015).
- [46] For the simple model here considered, the transverse-optical (TO) mode is harder than the longitudinal-optical (LO) mode, unlike the predictions of fully *ab-initio* calculations. This discrepancy does not affect the validity of the results of our analysis, with the simple warning that predictions for tensile strain might apply to compressive strain and vice-versa.
- [47] A. Molina-Sánchez, K. Hummer, and L. Wirtz, *Surf. Sci. Rep.* **70**, 554 (2015).
- [48] X. Zhang, X.-F. Qiao, W. Shi, J.-B. Wu, D.-S. Jiang, and P.-H. Tan, *Chem. Soc. Rev.* **44**, 2757 (2015).
- [49] R. Geick, C. H. Perry, and G. Rupprecht, *Phys. Rev.* **146**, 543 (1966).
- [50] S. Reich, A. C. Ferrari, R. Arenal, A. Loiseau, I. Bello, and J. Robertson, *Phys. Rev. B* **71**, 205201 (2005).
- [51] D. Sánchez-Portal and E. Hernández, *Phys. Rev. B* **66**, 235415 (2002).
- [52] Q. Cai, D. Scullion, A. Falin, K. Watanabe, T. Taniguchi, Y. Chen, E. J. G. Santos, and L. H. Li, *Nanoscale* **9**, 3059 (2017).